How to cite: *Angew. Chem. Int. Ed.* **2025**, *64*, e202415155
doi.org/10.1002/anie.202415155

MOFs in Catalysis

Location-Specific Microenvironment Modulation Around Single-Atom Metal Sites in Metal–Organic Frameworks for Boosting Catalysis

*Shuaishuai Hu[+], Jiajia Huang[+], Ming-Liang Gao, Zhongyuan Lin, Yunyang Qian, Weijie Yang, Long Jiao, and Hai-Long Jiang**

Abstract: Despite coordination environment of catalytic metal sites has been recognized to be of great importance in single-atom catalysts (SACs), a significant challenge remains in the understanding how the location-specific microenvironment in the higher coordination sphere influences their catalysis. Herein, a series of Cu-based SACs, namely Cu_1/UiO-66-X (X = -NO_2, -H, and -NH_2), are successfully constructed by anchoring single Cu atoms onto the Zr-oxo clusters of metal–organic frameworks (MOFs), i.e., UiO-66-X. The -X functional groups dangling on the MOF linkers could be regarded as location-specific remote microenvironment to regulate electronic properties of the single Cu atoms. Remarkably, they exhibit significant differences in the catalysis toward the hydroboration of alkynes. The activity follows the order of Cu_1/UiO-66-NO_2 > Cu_1/UiO-66 > Cu_1/UiO-66-NH_2 under identical reaction conditions, where Cu_1/UiO-66-NO_2 showcases the phenylacetylene conversion of 92%, ~3.5 times higher efficiency than that of Cu_1/UiO-66-NH_2. Experimental and calculation results jointly support that the Cu electronic structure is modulated by the location-specific microenvironment, thereby regulating the product desorption and promoting the catalysis.

Introduction

With the utmost atom utilization, single-atom catalysts (SACs) have captured intensive research interest toward various catalytic applications.[1] It has been well established that the first coordination sphere, including the specific atoms and the coordinated number, of catalytic metal sites in SACs play critical roles in the resulting catalytic performance.[2] Recently, a few studies have reported that the remote non-bonding heteroatoms and even their distance around catalytic metal sites are critical parameters for catalytic properties,[3] for example, the non-bonding carboxylate anions around catalytic Fe sites, serving as proton acceptors, could promote proton transfer and reduce the kinetic barrier for the formation of O–O bond.[3a] Although it has been recognized that the location-specific microenvironment modulation around catalytic metal sites in SACs is essential based on these scattered and limited findings, the accurate control of non-bonding heteroatoms and/or functional groups as surrounding microenvironment indeed remains a grand challenge. The main difficulty lies in the precise installation of the microenvironmental heteroatoms and/or functional groups, due to the random distribution of single metal atoms on conventional catalyst supports, such as porous carbons and metal oxides. Therefore, it is highly desired to find appropriate supports, in which the location of both catalytic metal sites and their location-specific group (serving as microenvironment) can be precisely controlled/regulated. To this end, the supports should meet the basic requirements: the well-defined structures (for precise location determination) and ease of structural tailorability at atomic level (for decoration of metal sites and/or groups).

With the above in mind, metal–organic frameworks (MOFs), emerging as crystalline porous materials with well-defined and tunable structures,[4] have been demonstrated to be very promising supports for stabilizing active metal sites, such as metal nanoparticles, toward heterogeneous catalysis.[5] Particularly, benefiting from the unique structural features of MOFs, it has been reported the decoration of single metal atoms onto Zr-oxo clusters with specific position.[6] Moreover, diverse functional groups can be readily furnished onto the linkers by a direct or post-synthetic modification way.[7] Meanwhile, the arrangement of metal clusters and organic linkers is periodic and predictable, leading to the tailorable microenvironmental groups with a fixed distance around single metal atoms. On this ground, MOFs could be ideal supports to precisely construct location-specific microenvironment around catalytic metal sites, so as to explore the corresponding structure-performance relationship in catalysis. Unfortunately, to our knowledge, location-specific microenviron-

[*] Dr. S. Hu,[+] Dr. J. Huang,[+] Dr. M.-L. Gao, Z. Lin, Dr. Y. Qian, Prof. Dr. L. Jiao, Prof. Dr. H.-L. Jiang
Hefei National Research Center for Physical Sciences at the Microscale, Department of Chemistry, University of Science and Technology of China, Hefei, Anhui 230026 (P. R. China)
E-mail: jianglab@ustc.edu.cn
Homepage: http://mof.ustc.edu.cn/
Dr. W. Yang
School of Energy and Power Engineering, North China Electric Power University, Baoding, Hebei 071003 (P. R. China)
[+] These authors contributed equally to this work.

ment modulation based on MOFs has not been reported for supported catalysts.

In this work, well-designed Cu_1/UiO-66-X (X=-NO_2, -H, and -NH_2) have been fabricated by anchoring single Cu atoms onto the Zr-oxo clusters in UiO-66-X via a rapid and facile microwave-assisted approach. The location-specific microenvironment surrounding the single Cu atoms is fine-tuned by dangling diverse functional groups on the linkers of UiO-66-X. Remarkably, Cu_1/UiO-66-X showcases much different activities in the hydroboration of phenylacetylene, in which the activity of Cu_1/UiO-66-NO_2 is ~3.5 times higher than that of Cu_1/UiO-66-NH_2. Both experimental and density functional theory (DFT) calculation results suggest that the electronic properties of Cu sites can be modulated by the location-specific -X groups. The lower Cu electron density, the easier desorption of the product, giving rise to the higher activity. To the best of our knowledge, this is the first report to investigate location-specific microenvironment modulation around single-atom metal sites in heterogeneous catalysis.

Results and Discussion

The representative MOFs of UiO-66-X, with the formula of $Zr_6O_4(OH)_4(BDC\text{-}X)_6$ (BDC = benzene-1,4-dicarboxylate, X=-NO_2, -H, and -NH_2), were synthesized using BDC-X and $ZrCl_4$, in the presence of acetic acid (CH_3COOH) as a modulator, under the solvothermal conditions.[8] Subsequently, a mixture of UiO-66-X and $Cu(acac)_2$ in methanol was treated by microwave-assisted process to afford Cu_1/UiO-66-X with similar Cu loadings of ~0.5 wt % (Scheme 1, Table S1). Powder X-ray diffraction (XRD) patterns show that the crystallinity of UiO-66-X is maintained after furnishing with Cu species (Figure S1). Compared to the parent MOFs (713–923 m^2/g), the Brunauer–Emmett–Teller (BET) surface area of Cu_1/UiO-66-X (616–880 m^2/g) is slightly reduced, which may be attributed to the mass occupancy of Cu sites (Figure S2).[9] The corresponding pore size distributions show that the characteristic pore structure can be well maintained after anchoring Cu sites. Scanning electron microscopy (SEM) and transmission electron microscopy (TEM) images reveal that Cu_1/UiO-66-X presents similar octahedral morphology to the parent MOFs, and no obvious Cu nanoparticles can be observed (Figures 1a–b, S3 and S4). The energy dispersive X-ray spectroscopy (EDS) mapping and the EDS line scan profile results for Cu_1/UiO-66-NO_2 as a representative support that the Cu species is well distributed throughout the Cu_1/UiO-66-NO_2 particle (Figures 1c-f and S5).

The specific location of the Cu sites was verified by using diffuse reflectance infrared Fourier transform spectroscopy (DRIFTS). The peak at 3671 cm^{-1} corresponds to the -OH/H_2O stretching peak in the Zr-oxo clusters. The noticeable decrease of peak intensity after anchoring Cu species to UiO-66-NO_2 indicates that Cu ions might coordinate with the -OH/H_2O on the Zr-oxo clusters (Figures 2a and S6), which supports the attachment of Cu sites onto Zr-oxo clusters of the MOFs.[2a] Additionally, the molar ratios of BDC-NO_2 and CH_3COO^- in UiO-66-NO_2 and Cu_1/UiO-66-NO_2 were determined by ^1H NMR upon their dissolution (Figures 2b and S7). The amount of CH_3COO^- significantly decreases after anchoring the Cu species, as evidenced by

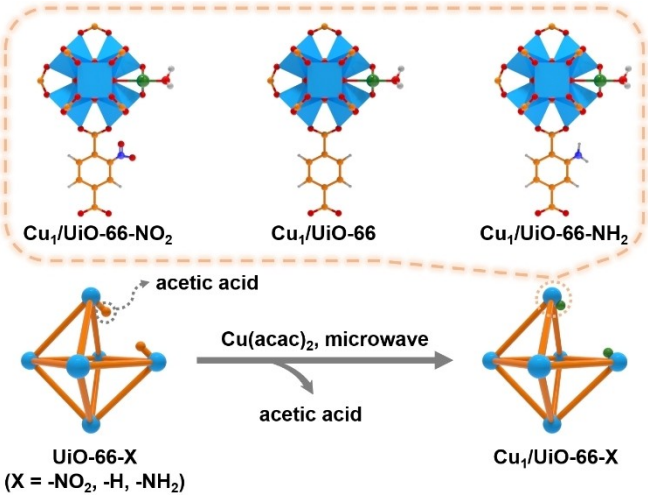

Scheme 1. Schematic showing the synthetic strategy for Cu_1/UiO-66-X (X=-NO_2, -H, and -NH_2).

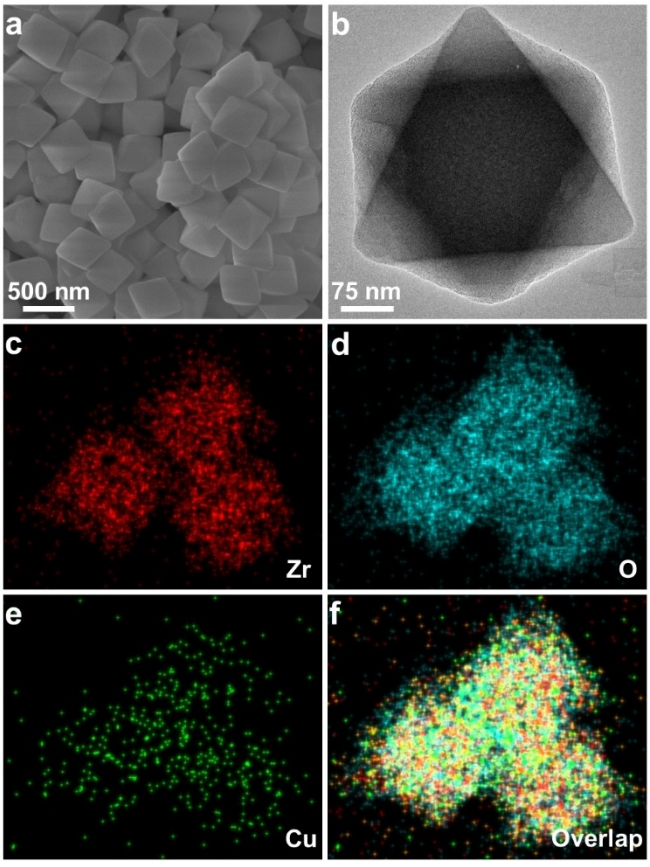

Figure 1. a) SEM and b) TEM images of Cu_1/UiO-66-NO_2. c-f) The corresponding EDS mapping of Zr, O, Cu elements, and their overlap in Cu_1/UiO-66-NO_2 as a representative.

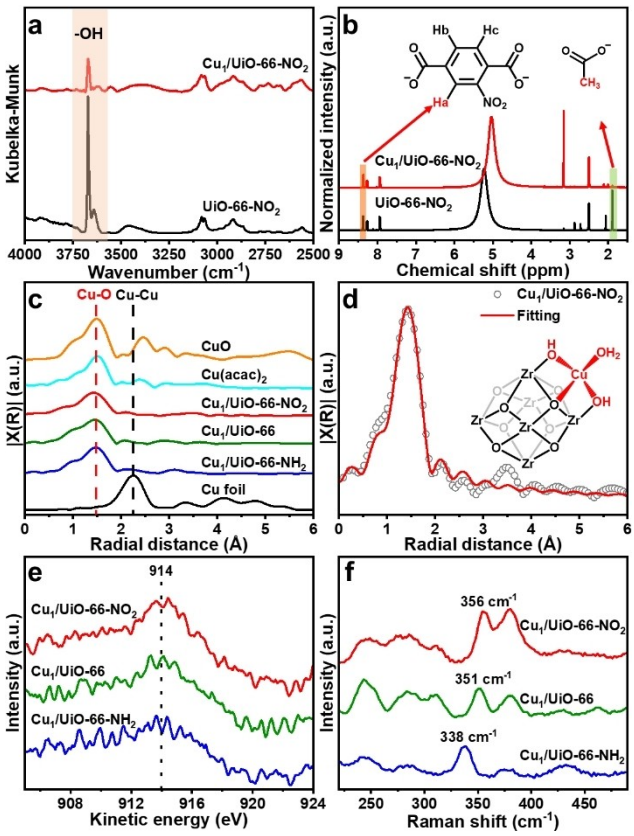

Figure 2. a) DRIFTS and b) ^{1}H NMR spectra of UiO-66-NO_2 and Cu_1/UiO-66-NO_2. c) EXAFS spectra of Cu_1/UiO-66-X (X=-NO_2, -H, and -NH_2), CuO, Cu(acac)$_2$, and Cu foil. d) EXAFS fitting of Cu_1/UiO-66-NO_2 (inset: proposed coordination structure of single Cu atom anchored on the Zr-oxo cluster). e) The AES spectra and f) Raman spectra of Cu_1/UiO-66-X (X=-NO_2, -H, and -NH_2).

reduced molar ratio of BDC-NO_2: CH_3COO^- from 1:0.43 to 1:0.04.[2a] Similar tendencies and results were also observed in UiO-66 and UiO-66-NH_2 upon introducing the Cu species (Figures S8–S12), demonstrating that CH_3COO^- on the Zr-oxo clusters is successfully substituted by the Cu sites.

X-ray absorption spectroscopy (XAS) has been conducted to investigate the existing form and coordination environment of Cu species. X-ray absorption near-edge spectroscopy (XANES) results reveal that the absorption edge for Cu_1/UiO-66-X lies at between those of Cu_2O and CuO (Figure S13) but more closer to Cu_2O, which suggests that the oxidation state for the Cu species may fall in the range from +1 to +2, and the +1 oxidation state would be dominant.[10] From the Fourier transform extended X-ray absorption fine structure (EXAFS) analysis, the appearance of dominant peak for all the Cu_1/UiO-66-X samples at ~1.5 Å (Cu–O bond) and the absence of peak at ~2.3 Å (Cu–Cu bond) suggest that the Cu species is in the existing form of single Cu atom (Figure 2c).[10] The fitting for EXAFS data of Cu_1/UiO-66-NO_2 reveals that one Cu atom is coordinated by four oxygen atoms, with average Cu–O bond length of ~1.93 Å (Figure 2d, Table S2). The Cu coordination environment in Cu_1/UiO-66 and Cu_1/UiO-66-NH_2 is similar with that in Cu_1/UiO-66-NO_2, with average Cu–O bond lengths of ~1.94 and ~1.95 Å, respectively (Figure S14, Table S2). Furthermore, the Auger electron spectra (AES) of Cu_1/UiO-66-X reveal that the peak at around 914 eV is attributed to Cu^+, with no peak corresponding to Cu^0 (Figure 2e), supporting the above assumption by XANES results.[11] Combined with the EXAFS results, it is assumed that the Cu species exists as single atoms rather than nanoparticles in Cu_1/UiO-66-X. The Raman spectra display characteristic peak in the range of 335–360 cm^{-1} assignable to the Cu–O bond (Figure 2f),[12] which further confirms the installation of single Cu atoms on the Zr-oxo clusters. The lower location of Raman peak reveals the lower frequency of vibration and the longer length of Cu–O bond, which reflects that the sequence of Cu–O bond lengths is Cu_1/UiO-66-NO_2 < Cu_1/UiO-66 < Cu_1/UiO-66-NH_2, in consistent with the above EXAFS results. All these results suggest that, both single-atom Cu sites and their surrounding -X groups are at well-defined positions, and even the distance between them is definite, in Cu_1/UiO-66-X.

Inspired by the above results, the catalytic hydroboration of phenylacetylene with Cu_1/UiO-66-X has been investigated. The hydroboration of alkynes is an effective route for the synthesis of vinylboranes that have a wide range of applications in drug synthesis, fine chemical engineering, etc.[13] To our delight, the conversion of phenylacetylene over Cu_1/UiO-66-NO_2 is up to 92 % with 91 % selectivity to the targeted *E*-phenylvinylboronate (Figure 3a, Table S3). Under the identical reaction conditions, the reaction

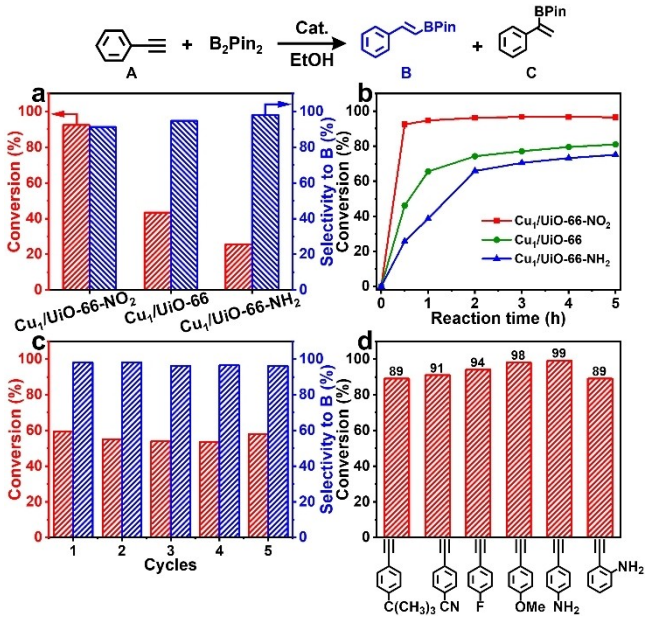

Figure 3. a) Conversion and selectivity in the catalytic hydroboration of phenylacetylene and b) time-dependent conversion of phenylacetylene hydroboration over Cu_1/UiO-66-X (X=-NO_2, -H, and -NH_2). c) Conversion and selectivity of five consecutive runs of reaction over Cu_1/UiO-66-NO_2. d) The hydroboration of phenylacetylene derivatives over Cu_1/UiO-66-NO_2. Reaction conditions: 10 mg catalyst, 0.1 mmol phenylacetylene, 0.3 mmol B_2Pin_2, 3 mL ethanol, 2 μL triethylamine, 85 °C, 0.5 h.

selectivities to *E*-phenylvinylboronate are similarly high of 95 % and 98 % for Cu_1/UiO-66 and Cu_1/UiO-66-NH_2, respectively. However, their conversions of phenylacetylene are relatively low to be 43 % and 26 %, respectively (Figure 3a, Table S3). With prolonged reaction time, the conversions over Cu_1/UiO-66 and Cu_1/UiO-66-NH_2 increase gradually (Figure 3b). Moreover, when BDC-NO_2 is mixed with BDC-NH_2 to fabricate the MOF in a multivariate approach, the resulting catalysts give gradually enhanced activity along with increased amount of BDC-NO_2 (Figure S15), in consistence with the above observation. The results highlight the critical roles of location-specific -X groups surrounding single Cu atoms in the catalysis. In the absence of catalyst or the present of UiO-66-X, the activity is negligible, inferring that the Cu species is the real active site in the reaction (Table S3). Furthermore, Cu_1/UiO-66-NO_2 exhibits higher activity than all other counterparts (Table S3), indicating that single-atom Cu sites on Zr-oxo clusters are favorable to the activity. In addition, the activity of phenylacetylene conversion and its selectivity to *E*-phenylvinylboronate are well maintained during five cycles (Figure 3c). The crystallinity, morphology, and the loading of Cu can be retained after the reaction, confirming the stability of Cu_1/UiO-66-NO_2 (Figures S16 and S17, Table S1).

Encouraged by the excellent catalytic performance of Cu_1/UiO-66-NO_2 in the hydroboration of phenylacetylene, various substituted phenylacetylenes have been examined to demonstrate its general applicability (Figure 3d). To our delight, all the substituted phenylacetylenes, with both electron-withdrawing and -donating groups, exhibit outstanding activities under the identical conditions (89–99 %). The superior activities of the diverse substituted phenylacetylene derivatives reveal the general applicability of Cu_1/UiO-66-NO_2. The conversion rate of 4-ethynylphenylamine reaches 99 % within 0.5 h, slightly higher than that of phenylacetylene (92 %), which might be attributed to the electronic effect. However, the conversion rates of 2-ethynylphenylamine and 4-(tert-butyl)phenylethynyl are both slightly lower at 89 %. This may be due to the steric hindrance in these two phenyl derivatives. The comparative analysis reveals that the sizes of phenylacetylene and its derivatives are smaller than the MOF pore size, indicating that the reaction can occur in the MOF pores (Figures S18). Additional substrate diffusion experiments are consistant with this result. (Figures S19).[14]

To understand the catalytic activity differences among Cu_1/UiO-66-X (X=-NO_2, -H, and -NH_2), the electronic structures of single Cu atoms in these catalysts have been studied. X-ray photoelectron spectroscopy (XPS) and AES results show that the XPS peaks at 932–934 and 952–954 eV for Cu_1/UiO-66-X can be ascribed to $2p_{3/2}$ and $2p_{1/2}$ of Cu^+, respectively (Figures 2e and 4a).[11,15] The sequence of electronic binding energies for Cu 2p is Cu_1/UiO-66-NO_2 > Cu_1/UiO-66 > Cu_1/UiO-66-NH_2, which is in agreement with the activity trend, corresponding to electron-deficiency character of the Cu species in them (electron-withdrawing ability: -NO_2 > -H > -NH_2). The difference in the Cu electronic properties might be responsible for the differentiated activity. To further assess the influence of the location-specific -X groups on the electronic properties of Cu sites, soft X-ray absorption spectroscopy (sXAS) has been performed. There are two primary peaks, corresponding to the orbital transitions from $2p_{3/2}$ to 3d (L_3) and from $2p_{1/2}$ to 3d (L_2), respectively (Figure 4b).[16] Compared to those of Cu_1/UiO-66-NO_2, the peaks of L_3 and L_2 for Cu_1/UiO-66 and Cu_1/UiO-66-NH_2 shift to a lower energy region, indicating the Cu electronic density tendency of Cu_1/UiO-66-NO_2 < Cu_1/UiO-66 < Cu_1/UiO-66-NH_2. Moreover, the CO-DRIFTS spectra display the main adsorption peaks between 2000–2200 cm^{-1} attributed to the C–O vibrations of linear CO-adsorption (Figure 4c).[9] The main peaks appear at 2113, 2106, and 2097 cm^{-1} for Cu_1/UiO-66-NO_2, Cu_1/UiO-66, and Cu_1/UiO-66-NH_2, respectively, manifesting the electron-donating capability of the surrounding -X group around Cu sites: -NO_2 < -H < -NH_2,[9] which is in line with the XPS results (Figure 4a). In addition, the charge model 5 (CM5) analyses by DFT calculations also verify electron transfer from single Cu atoms to UiO-66-NO_2, UiO-66, and UiO-66-NH_2 are 1.393, 1.347, and 1.335 *e*, respectively (Figures 4d and S20).[17] All above experimental and calculation results corroborate each other, jointly demonstrating that the electron effect from modulated location-specific microenvironment (the -X group) gives rise to the discriminative Cu electron density, accounting for the different activity.

Given both ethanol and H_2O are possible hydrogen sources for the hydroboration of alkynes from the previous reports,[18] deuterium labeling experiments using ethanol-d_1 and D_2O as the reaction solvents have been conducted, respectively (Figure S21). When using the mixed solvents of ethanol-d_1 and H_2O, the deuterium atom can not be detected in the *E*-phenylvinylboronate product (m/z = 230). By contrast, with mixed solvents of extra dry ethanol and

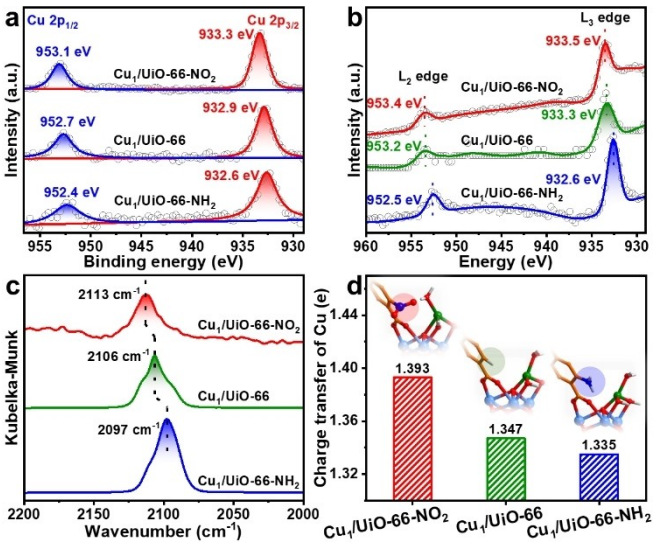

Figure 4. The a) XPS, b) Cu L-edge sXAS, and c) CO-DRIFTS spectra of Cu_1/UiO-66-X (X=-NO_2, -H, and -NH_2). d) The calculated number of electron transfer from Cu to the -X group in Cu_1/UiO-66-X (X=-NO_2, -H, and -NH_2).

D_2O, the deuterium hydrogen atom of D_2O is transferred to the *E*-phenylvinylboronate (m/z = 231).[18a] Moreover, the reaction activity is much different in altered solvents of ethanol, H_2O, or their mixed solvents (Table S4). The activity is the lowest one with using extra dry ethanol as the solvent, and gradually increases with more H_2O ratio. The results suggest that H_2O in ethanol is the hydrogen source for the hydroboration of alkynes, as further supported by ^{11}B NMR spectrum (Figure S22), where more HOBPin can be observed by introducing an increased amount of H_2O in the solvent. The tendency indicates that H_2O could facilitate the decomposition of bis(pinacolato)diboron (B_2Pin_2) to form HBPin and HOBPin as intermediate products.[19] The absence of the hydrolysis product HBPin in ^{11}B NMR spectra might be ascribed to its difficulty of being detected and ease of spontaneous degradation to HOBPin.[20] As a matter of fact, HBPin can be directly adopted for the hydroboration of phenylacetylene, as reported in a previous report.[19a] In addition, the amount of HOBPin product significantly increases upon the addition of triethylamine (Figure S23), demonstrating that triethylamine is able to promote the hydrolysis of B_2Pin_2.

DFT calculations have been further carried out to simulate the catalytic pathway and evaluate the corresponding Gibbs free energy in the hydroboration of phenylacetylene (Figure 5).[13a,18a] At the beginning, B_2Pin_2 dissociates to HOBPin and HBPin in the presence of TEA and H_2O, with HBPin adsorbed onto Zr-oxo clusters to form *HBPin. Meanwhile, HBPin decomposes to BPin unit and H' atom that are adsorbed on the Cu_1 site and -OH group on Zr-oxo cluster, respectively (Figure S24). Then, the *β*-carbon atom of phenylacetylene is also attached onto the Cu_1 site after adsorption with the formation of *HBPin-Ph-CCH (*β*) (Figure S25). Afterwards, with the combination of BPin and phenylacetylene, the B atom of BPin bonds with the *β*-carbon atom of phenylacetylene. Subsequently, upon the combination of BPin unit and phenylacetylene, *HBPin-Ph-CCH (*α*) is formed (Figure S26). In *HBPin-Ph-CCH (*α*), B atom bonds to *β*-carbon atom, while both *α*- and *β*-carbon atoms link to Cu_1 site, and the configuration of phenylacetylene is slightly distorted. Upon the addition of H' (originated from HBPin and then bonded with -OH group from Zr-oxo cluster prior to this step) to the *α*-carbon atom of phenylacetylene, the product of *E*-phenylvinylboronate is generated (Figure S27). Finally, the *E*-phenylvinylboronate desorbs from the Cu_1 site, which is the rate-determining step (RDS) (Figure S28). The corresponding ΔG values of RDS are 0.723, 0.789, and 0.828 eV for Cu_1/UiO-66-NO_2, Cu_1/UiO-66, and Cu_1/UiO-66-NH_2, respectively (Figure 5). The calculation results align with the sequence of experimentally observed activity: Cu_1/UiO-66-NO_2 > Cu_1/UiO-66 > Cu_1/UiO-66-NH_2. Meanwhile, a possible reaction mechanism can be proposed based on the above results (Figure S29). Overall, the location-specific functional groups as microenvironment of single Cu atoms regulate the Cu electronic properties in Cu_1/UiO-66-X, which affects the desorption of product from the single Cu site, contributing to discrepancy of the resulting activity.

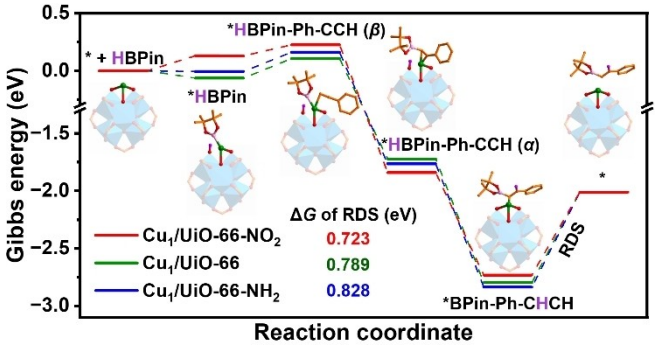

Figure 5. The potential reaction pathway and the corresponding Gibbs free energy for the hydroboration of phenylacetylene over Cu_1/UiO-66-X (X = -NO_2, -H, and -NH_2).

Conclusion

In summary, a series of Cu SACs, Cu_1/UiO-66-X (X = -NO_2, -H, and -NH_2) featuring Cu_1 sites surrounding with modulated microenvironment of location-specific -X groups, have been deliberately fabricated for efficient and selective hydroboration of phenylacetylene. They provide ideal models with the only variable of the -X functional group on the linker to investigate how the location-specific remote microenvironment affects the catalysis. Remarkably, Cu_1/UiO-66-NO_2 showcases ~2.1 and ~3.5 times higher activity than that of Cu_1/UiO-66 and Cu_1/UiO-66-NH_2, respectively. Experimental and theoretical results jointly demonstrate that the remote microenvironment of location-specific -X groups around Cu sites plays a critical role in the regulation of the Cu electronic properties, which gives rise to the low Cu electron density in Cu_1/UiO-66-NO_2 and influences the desorption capability of product, and ultimately boosting its activity. This study, for the first time, discloses how the location-specific microenvironment around catalytic metal sites affects the catalysis based on MOF platform. The results obtained herein would open a new avenue to the design and synthesis of heterogeneous catalysts by means of location-specific microenvironment modulation for enhanced performance.

Acknowledgements

This project was supported by the National Key Research and Development Program of China (2021YFA1500402), the National Natural Science Foundation of China (22331009, 22101269), the Strategic Priority Research Program of the Chinese Academy of Sciences (XDB0450302, XDB0540000), and the Postdoctoral Fellowship Program of CPSF (GZC20232532). We thank the 1W1B station at the BSRF for their support in conducting XAS measurements and BL10B at the NSRL for L-edge sXAS measurements. The calculations in this work are supported by the Supercomputing Center of the University of Science and Technology of China (USTC) and Hefei Advanced Computing

Center. This work was partially carried out at the Instruments Center for Physical Science, USTC.

Conflict of Interest

The authors declare no conflict of interest.

Data Availability Statement

The data that support the findings of this study are available from the corresponding author upon reasonable request.

Keywords: metal–organic frameworks · copper · single atom · heterogeneous catalysis · microenvironment modulation

[1] a) B. Qiao, A. Wang, X. Yang, L. F. Allard, Z. Jiang, Y. Cui, J. Liu, J. Li, T. Zhang, *Nat. Chem.* **2011**, *3*, 634–641; b) Z. Li, S. Ji, Y. Liu, X. Cao, S. Tian, Y. Chen, Z. Niu, Y. Li, *Chem. Rev.* **2020**, *120*, 623–682; c) C. Tang, Y. Jiao, B. Shi, J.-N. Liu, Z. Xie, X. Chen, Q. Zhang, S.-Z. Qiao, *Angew. Chem. Int. Ed.* **2020**, *59*, 9171–9176; *Angew. Chem.* **2020**, *132*, 9256–9261; d) V. Giulimondi, S. Mitchell, J. Pérez-Ramírez, *ACS Catal.* **2023**, *13*, 2981–2997.

[2] a) X. Ma, H. Liu, W. Yang, G. Mao, L. Zheng, H.-L. Jiang, *J. Am. Chem. Soc.* **2021**, *143*, 12220–12229; b) J. L. Fiorio, M. A. S. Garcia, M. L. Gothe, D. Galvan, P. C. Troise, C. A. Conte-Junior, P. Vidinha, P. H. C. Camargo, L. M. Rossi, *Coord. Chem. Rev.* **2023**, *481*, 215053; c) Y. Zhang, L.-Z. Dong, S. Li, X. Huang, J.-N. Chang, J.-H. Wang, J. Zhou, S.-L. Li, Y.-Q. Lan, *Nat. Commun.* **2021**, *12*, 6390; d) Y.-S. Wei, M. Zhang, R. Zou, Q. Xu, *Chem. Rev.* **2020**, *120*, 12089–12174; e) Y. Li, S. Zuo, F. Wei, C. Chen, G. Zhang, X. Zhao, Z. Wu, S. Wang, W. Zhou, M. Rueping, Y. Han, H. Zhang, *Proc. Natl. Acad. Sci. USA* **2024**, *121*, e2315362121.

[3] a) M. Liu, N. Li, X. Wang, J. Zhao, D.-C. Zhong, W. Li, X.-H. Bu, *Angew. Chem. Int. Ed.* **2023**, *62*, e202300507; *Angew. Chem.* **2023**, *135*, e202300507; b) T. Islamoglu, M. A. Ortuño, E. Proussaloglou, A. J. Howarth, N. A. Vermeulen, A. Atilgan, A. M. Asiri, C. J. Cramer, O. K. Farha, *Angew. Chem. Int. Ed.* **2018**, *57*, 1949–1953; *Angew. Chem.* **2018**, *130*, 1967–1971; c) Y. Guo, W. Shi, H. Yang, Q. He, Z. Zeng, J.-Y. Ye, X. He, R. Huang, C. Wang, W. Lin, *J. Am. Chem. Soc.* **2019**, *141*, 17875–17883; d) W. Xu, Y. Wu, W. Gu, D. Du, Y. Lin, C. Zhu, *Chem. Soc. Rev.* **2024**, *53*, 137–162.

[4] a) H. Furukawa, K. E. Cordova, M. O'Keeffe, O. M. Yaghi, *Science* **2013**, *341*, 1230444; b) H.-C. J. Zhou, S. Kitagawa, *Chem. Soc. Rev.* **2014**, *43*, 5415–5418; c) A. Ebadi Amooghin, H. Sanaeepur, R. Luque, H. Garcia, B. Chen, *Chem. Soc. Rev.* **2022**, *51*, 7427–7508; d) S. Horike, S. Kitagawa, *Nat. Mater.* **2022**, *21*, 983–985; e) A. N. Hong, H. Yang, X. Bu, P. Feng, *EnergyChem* **2022**, *4*, 100080; f) L. Jiao, H.-L. Jiang, *Chin. J. Catal.* **2023**, *45*, 1–5.

[5] a) Q. Yang, Q. Xu, H.-L. Jiang, *Chem. Soc. Rev.* **2017**, *46*, 4774–4808; b) L. Li, Z. Li, W. Yang, Y. Huang, G. Huang, Q. Guan, Y. Dong, J. Lu, S.-H. Yu, H.-L. Jiang, *Chem* **2021**, *7*, 686–698; c) K. L. Kollmannsberger, L. Kronthaler, J. R. Jinschek, R. A. Fischer, *Chem. Soc. Rev.* **2022**, *51*, 9933–9959; d) M. Mukoyoshi, H. Kitagawa, *Chem. Commun.* **2022**, *58*, 10757–10767; e) J. Chen, Y. Wang, F. Wang, Y. Li, *Angew. Chem. Int. Ed.* **2023**, *62*, e202218115; *Angew. Chem.* **2023**, *135*, e202218115; f) W. Zhang, J. Wu, W. Shi, P. Qin, W. Lang, X. Zhang, Z. Gu, H. Li, Y. Fan, Y. Shen, S. Zhang, Z. Liu, Y. Fu, W. Zhang, F. Huo, *Adv. Mater.* **2023**, *35*, 2303216; g) G. Li, S. Zhao, Y. Zhang, Z. Tang, *Adv. Mater.* **2018**, *30*, 1800702.

[6] a) K. Manna, P. Ji, Z. Lin, F. X. Greene, A. Urban, N. C. Thacker, W. Lin, *Nat. Commun.* **2016**, *7*, 12610; b) X. Wang, X. Zhang, P. Li, K.-i. Otake, Y. Cui, J. Lyu, M. D. Krzyaniak, Y. Zhang, Z. Li, J. Liu, C. T. Buru, T. Islamoglu, M. R. Wasielewski, Z. Li, O. K. Farha, *J. Am. Chem. Soc.* **2019**, *141*, 8306–8314; c) A. M. Abdel-Mageed, B. Rungtaweevoranit, M. Parlinska-Wojtan, X. Pei, O. M. Yaghi, R. J. Behm, *J. Am. Chem. Soc.* **2019**, *141*, 5201–5210; d) C. Xu, Y. Pan, G. Wan, H. Liu, L. Wang, H. Zhou, S.-H. Yu, H.-L. Jiang, *J. Am. Chem. Soc.* **2019**, *141*, 19110–19117; e) G. Fang, F. Wei, J. Lin, Y. Zhou, L. Sun, X. Shang, S. Lin, X. Wang, *J. Am. Chem. Soc.* **2023**, *145*, 13169–13180.

[7] a) X. Mao, W. Gong, Y. Fu, J. Li, X. Wang, A. P. O'Mullane, Y. Xiong, A. Du, *J. Am. Chem. Soc.* **2023**, *145*, 21442–21453; b) X. Liao, X. Wang, F. Wang, Y. Yao, S. Lu, *J. Inorg. Organomet. Polym. Mater.* **2021**, *31*, 756–762; c) M. Kandiah, M. H. Nilsen, S. Usseglio, S. Jakobsen, U. Olsbye, M. Tilset, C. Larabi, E. A. Quadrelli, F. Bonino, K. P. Lillerud, *Chem. Mater.* **2010**, *22*, 6632–6640.

[8] a) J. H. Cavka, S. Jakobsen, U. Olsbye, N. Guillou, C. Lamberti, S. Bordiga, K. P. Lillerud, *J. Am. Chem. Soc.* **2008**, *130*, 13850–13851; b) T. He, X. Xu, B. Ni, H. Wang, Y. Long, W. Hu, X. Wang, *Nanoscale* **2017**, *9*, 19209–19215.

[9] G. Yang, D. Wang, Y. Wang, W. Hu, S. Hu, J. Jiang, J. Huang, H.-L. Jiang, *J. Am. Chem. Soc.* **2024**, *146*, 10798–10805.

[10] A. M. Abdel-Mageed, B. Rungtaweevoranit, S. Impeng, J. Bansmann, J. Rabeah, S. Chen, T. Häring, S. Namuangrak, K. Faungnawakij, A. Brückner, R. J. Behm, *Angew. Chem. Int. Ed.* **2023**, *62*, e202301920; *Angew. Chem.* **2023**, *135*, e202301920.

[11] J. Feng, L. Zhang, S. Liu, L. Xu, X. Ma, X. Tan, L. Wu, Q. Qian, T. Wu, J. Zhang, X. Sun, B. Han, *Nat. Commun.* **2023**, *14*, 4615.

[12] a) Y. Deng, A. D. Handoko, Y. Du, S. Xi, B. S. Yeo, *ACS Catal.* **2016**, *6*, 2473–2481; b) Z. Fan, Q. Yang, W. Zhang, H. Wen, H. Yuan, J. He, H. G. Yang, Z. Chen, *Nano Lett.* **2023**, *23*, 11314–11322.

[13] a) W.-H. Li, J. Yang, H. Jing, J. Zhang, Y. Wang, J. Li, J. Zhao, D. Wang, Y. Li, *J. Am. Chem. Soc.* **2021**, *143*, 15453–15461; b) R.-J. Wei, P.-Y. You, H. Duan, M. Xie, R.-Q. Xia, X. Chen, X. Zhao, G.-H. Ning, A. I. Cooper, D. Li, *J. Am. Chem. Soc.* **2022**, *144*, 17487–17495; c) W. Zhu, S. Zhang, W. Fan, Y. Yang, H. Zhao, W. Fei, H. Bi, J. He, M.-B. Li, *Precis. Chem.* **2023**, *1*, 175–182.

[14] a) J. T. Bryant, M. W. Logan, Z. Chen, M. Djokic, D. R. Cairnie, D. A. Vazquez-Molina, A. Nijamudheen, K. R. Langlois, M. J. Markley, G. Pombar, A. A. Holland, J. D. Caranto, J. K. Harper, A. J. Morris, J. L. Mendoza-Cortes, T. Jurca, K. W. Chapman, F. J. Uribe-Romo, *J. Am. Chem. Soc.* **2023**, *145*, 4589–4600; b) F. Gao, R. Yan, Y. Shu, Q. Cao, L. Zhang, *RSC Adv.* **2022**, *12*, 10114–10125.

[15] Y. Li, Z. Wang, C. Li, F. Qi, P. Yan, Y. Wang, M. He, Z. Chen, Q. Wang, Y. Wang, H. Zheng, A. Ikhlaq, J. Kumirska, E. Maria Siedlecka, O. Ismailova, *Chem. Eng. J.* **2023**, *470*, 144387.

[16] a) Y.-Y. Liu, H.-L. Zhu, Z.-H. Zhao, N.-Y. Huang, P.-Q. Liao, X.-M. Chen, *ACS Catal.* **2022**, *12*, 2749–2755; b) Q. Wang, Y. Zhang, M. Lin, H. Wang, Y. Bai, C. Liu, J. Lu, Q. Luo, G. Wang, H.-L. Jiang, T. Yao, X. Zheng, *Adv. Energy Mater.* **2023**, *13*, 2302692.

[17] A. V. Marenich, S. V. Jerome, C. J. Cramer, D. G. Truhlar, *J. Chem. Theory Comput.* **2012**, *8*, 527–541.

[18] a) L. J. Zhang, J. C. Yuan, L. J. Ma, Z. Y. Tang, X. M. Zhang, *J. Catal.* **2021**, *401*, 63–69; b) Z. Zhang, X. Ma, Y. Li, N. Ma, M.

Wang, W. Liu, J. Peng, Y. Liu, Y. Li, *J. Am. Chem. Soc.* **2024**, *146*, 8425–8434.

[19] a) S. B. Thorpe, J. A. Calderone, W. L. Santos, *Org. Lett.* **2012**, *14*, 1918–1921; b) Y. Yuan, F.-P. Wu, X.-F. Wu, *Chem. Sci.* **2021**, *12*, 13777–13781; c) Y. Pang, M. Leutzsch, N. Nöthling, J. Cornella, *J. Am. Chem. Soc.* **2020**, *142*, 19473–19479.

[20] A. J. Lyons, A. Clarke, H. Fisk, B. Jackson, P. R. Moore, S. Oke, T. O. Ronson, R. E. Meadows, *Org. Process Res. Dev.* **2022**, *26*, 1378–1388.

Manuscript received: August 8, 2024
Accepted manuscript online: November 7, 2024
Version of record online: November 19, 2024